Journal of Power Sources 249 (2014) 418–430

Contents lists available at ScienceDirect

Journal of Power Sources

journal homepage: www.elsevier.com/locate/jpowsour

Modelling of operation of a lithium-air battery with ambient air and oxygen-selective membrane

Ukrit Sahapatsombut [a,b,*], Hua Cheng [b], Keith Scott [b]

[a] National Metal and Materials Technology Center (MTEC), 114 Thailand Science Park, Paholyothin Rd., Klong Luang, Pathumthani 12120, Thailand
[b] School of Chemical Engineering and Advanced Materials, Newcastle University, Merz Court, Newcastle upon Tyne NE1 7RU, UK

HIGHLIGHTS

- A macro-homogeneous model is developed to operate Li-air battery in ambient air.
- The Li-air model is combined with an oxygen-selective membrane.
- The model shows the battery deterioration when using air.
- The Li-air performance increases with integration of oxygen-selective membrane.

ARTICLE INFO

Article history:
Received 17 July 2013
Received in revised form
1 October 2013
Accepted 24 October 2013
Available online 5 November 2013

Keywords:
Rechargeable
Li-air battery
Macro-homogeneous model
Ambient air operation
Discharge products
Oxygen-selective membrane

ABSTRACT

A macro-homogeneous model has been developed to evaluate the impact of replacing pure oxygen with ambient air on the performance of a rechargeable non-aqueous Li-air battery. The model exhibits a significant reduction in discharge capacity, e.g. from 1240 to 226 mAh g^{-1}_{carbon} at 0.05 mA cm^{-2} when using ambient air rather than pure oxygen. The model correlates the relationship between the performance and electrolyte decomposition and formation of discharge products (such as Li_2O_2 and Li_2CO_3) under ambient air conditions. The model predicts a great benefit of using an oxygen-selective membrane on increasing capacity. The results indicate a good agreement between the experimental data and the model.

1. Introduction

Several times higher specific energy than Li-ion batteries makes the rechargeable Li-air a candidate of new generation of energy storage devices [1–4]. Since the first report of a non-aqueous electrolyte Li-air battery in 1996 [5], especially after a breakthrough in cycle life by Bruce's group [6], the rechargeable Li-air battery has been investigated intensively [6–11]. However, many science and technical challenges have to be overcome to realise the potential of this cutting-edge technology. A key area is to gain insights into chemical/electrochemical processes that take place inside the Li-air battery via an effective modelling.

An aprotic Li-air battery contains a metal lithium anode, a solid separator and a porous air electrode filled with a non-aqueous Li^+ electrolyte. The fundamental electrochemical reactions are shown below:

$$\text{Anode}: \text{Li(metal)} \leftrightarrow \text{Li}^+ + \text{e}^- \left(E_{\text{ref}} = 0\ \text{V}\right) \quad \text{(I)}$$

$$\text{Cathode}: 2\text{Li}^+ + \text{O}_2 + 2\text{e}^- \leftrightarrow (\text{Li}_2\text{O}_2)_{\text{solid}} (E_{\text{rev}} = 2.96\ \text{V vs Li}) \quad \text{(II)}$$

Here, Eq. (II) is an ideal electrochemical reaction, desired to make a truly rechargeable Li-air battery [6,12,13]. In practice, there are other side reactions, forming detrimental products, such as Li_2CO_3 [6,12,13].

However, almost all the current studies of Li-air batteries are run in pure oxygen and controlled a dried atmosphere in a glove box to minimise the contaminated substances from ambient air, thus this

* Corresponding author. National Metal and Materials Technology Center (MTEC), 114 Thailand Science Park, Paholyothin Rd., Klong Luang, Pathumthani 12120, Thailand. Tel.: +66 2564 6500; fax: +66 2564 6403.
E-mail addresses: ukrit.sahapatsombut@ncl.ac.uk, ukrits@mtec.or.th (U. Sahapatsombut).

0378-7753/$ – see front matter © 2013 Elsevier B.V. All rights reserved.
http://dx.doi.org/10.1016/j.jpowsour.2013.10.128

battery can perform in high rate capability, owing to high oxygen concentration, and maintain the long-term operation. Our recent model studies also simulated the Li-air battery including the electrolyte degradation and operating in pure oxygen [14,15]. To success in making a Li-air battery for use in practical applications, one critical problem to be solved is operating Li-air batteries in ambient air environment [16,17]. There are several challenges when Li-air batteries are applied with air condition comparing to those of pure oxygen feeding. The first is unavoidable moisture (about 1% in volume) in surrounding air, which may penetrate into the cell system together with oxygen. The present of moisture can corrode the metallic lithium anode due to the hydrolysis reaction with highly reactive lithium as shown in reaction III [17]. This results in the fast battery failure and causes a serious safety issues.

$$2Li + 2H_2O \leftrightarrow 2LiOH + H_2 \quad \text{(III)}$$

The second is the insufficient concentration of oxygen due to its low partial pressure in atmosphere, leading to limit Li-air batteries from high discharge rates because of small oxygen solubility in the electrolyte. The third problem is that the small amount of carbon dioxide (CO_2) from air feeding may react with superoxide anions, which is formed during the initial oxygen reduction on discharge process, to generate carbonate species, leading to the deposition of these by-products on the cathode surface [12,18,19]. It is worth noting that CO_2 could be considered as the active material to form the Li_2CO_3 and lithium alkyl carbonates instead of desired produce Li_2O_2 [12,19,20]. Furthermore, these side reactions lead to continuous and irreversible consumption of electrolytes and thus the Li-air batteries cannot maintain their sustainable ability during charge/discharge cycles.

To minimise the battery problem when using air, Li-air batteries under current research are mainly operated in pure oxygen [5–7,9]. There is a small volume of published works demonstrating the behaviour of Li-air battery with air feeding [11,16,17,21]. These studies solved the contaminated gases problems by using an oxygen-selective water barrier membrane covering the outer surface of the cathode to prevent moisture and permeate oxygen into the porous cathode at the same time. Zhang et al. developed an oxygen-selective immobilised liquid membrane for a non-aqueous Li-air battery operated in ambient air with 20–30% relative humidity [17]. The membranes were easily prepared by soaking high viscosity silicone oil into porous metal or Teflon substrates. A Li-air integrated with these membranes can be operated in ambient air for 16.3 days with a specific capacity of 789 mAh g^{-1} and specific energy of 2182 Wh kg^{-1} based on the weight of carbon. The same group also studied the hydrophobic zeolite membrane and poly(-tetrafluoroethylene) (PTFE) membrane as oxygen-selective water barriers [16]. The latter protected a Li-air against moisture and supplied oxygen for 21 day with a specific capacity of 1022 mAh g^{-1} and specific energy of 2792 Wh kg^{-1} based on the weight of carbon.

Zhang et al. investigated the ambient operation of non-aqueous Li-air batteries integrating with a heat-sealable polymer membrane to serve as both an oxygen-diffusion membrane and moisture barrier [11]. The membrane could also reduce the evaporation of electrolytes during battery operation. The Li-air battery with this membrane demonstrated the discharge capability in ambient air for more than one month with a specific energy of 362 Wh kg^{-1} based on the total weight of the battery including its packaging. However, all the previously mentioned ambient air works only studied the Li-air performances on discharge phase without showing those on charging or cycling process, which could provide more important data for battery stability than only single discharge.

In this paper our previous Li-air model with electrolyte degradation is modified to operate the Li-air battery in ambient air environment [14,15], which severely damages Li-air performance and is still a critical problem to be solved before the Li-air battery can be used for practical application. The two species of oxygen and CO_2 are considered in the model as air feeding condition with the exception of moisture or using dried air in the model. Although this model does not include all the effects that could occur in the Li-air battery with ambient air operation, at least we carefully consider the key mechanisms covering the main impacts of using air that directly affect the porous cathode behaviour during cell operation, leading to detrimental cell performance. Therefore, mathematical model for Li-air battery with air feeding condition can be used to identify cell-limiting mechanisms and reduce the time-consuming work compared to experiment aspect. Moreover, it also avoids the serious safety problems that could happen when the ingress of moisture reacts with lithium metal anode. This model can be used to describe the behaviour of Li-air batteries in ambient air condition as well as to optimise the performance and structure of these battery electrodes.

2. Theoretical mechanism analysis

A typical Li-air battery, shown in Fig. 1a, contains a lithium metal anode, a separator containing electrolyte, and a porous carbon or catalyst-loaded carbon air electrode filled with an organic electrolyte comprising a dissolved lithium salt in an aprotic solvent. During discharge the lithium metal anode oxidises to Li^+ and electrons conduct through the external circuit, while Li^+ transports towards the porous cathode. Oxygen is reduced at the active surface with Li^+, thus leading to the desired discharge products of Li_2O_2 and the by-product of Li_2CO_3 or lithium alkyl carbonates resulting from the electrolyte decomposition [12,13,19]. These products influenced the Li-air performance and cannot completely remove during battery cycling. To simplify our simulation, the model assumed that Li_2O_2 was the main discharge product depositing inside the porous cathode (Eq. (II)) and the irreversible Li_2CO_3 by-product coexisting with Li_2O_2 when using non-aqueous electrolytes. This section describes the two main mechanisms that occur inside the Li-air battery and were applied to the model.

2.1. Effect of using ambient air condition

The critical problems when using air as a feeding reactant for the Li-air battery are the low oxygen solubility in the electrolyte and the CO_2 gas diffusing into the battery with oxygen. To investigate these effects, the Li-air model was changed the feeding condition from pure oxygen to ambient air at the porous cathode entrance. Considering the amount of oxygen and CO_2 content in the atmosphere [22] (78% N_2, 21% O_2, 0.035% CO_2), the concentration of oxygen and CO_2 in the electrolyte can be determined in term of Henry's law which states that

$$c_g = H_g \overline{p}_g \quad (1)$$

where c_g is the concentration of gasses in the electrolyte, H_g is the Henry's law constant which depends on the electrolyte and temperature used in the Li-air battery, and $\overline{p}_g$ is the partial pressure of the gas which depends on mole fraction of each specie in the atmosphere. Henry's law is correct to describe the solubility of gas for low concentrations and low partial pressures. The concentrations of oxygen and CO_2 calculated from Henry's law can be compared in Table 1. These concentrations are applied in the Li-air model to represent the air feeding condition, unless specified otherwise. It can be seen that although the CO_2 composition is not much in the atmosphere, its Henry's law constant is almost two times higher than that of oxygen, i.e. the solubility of CO_2 in non-aqueous

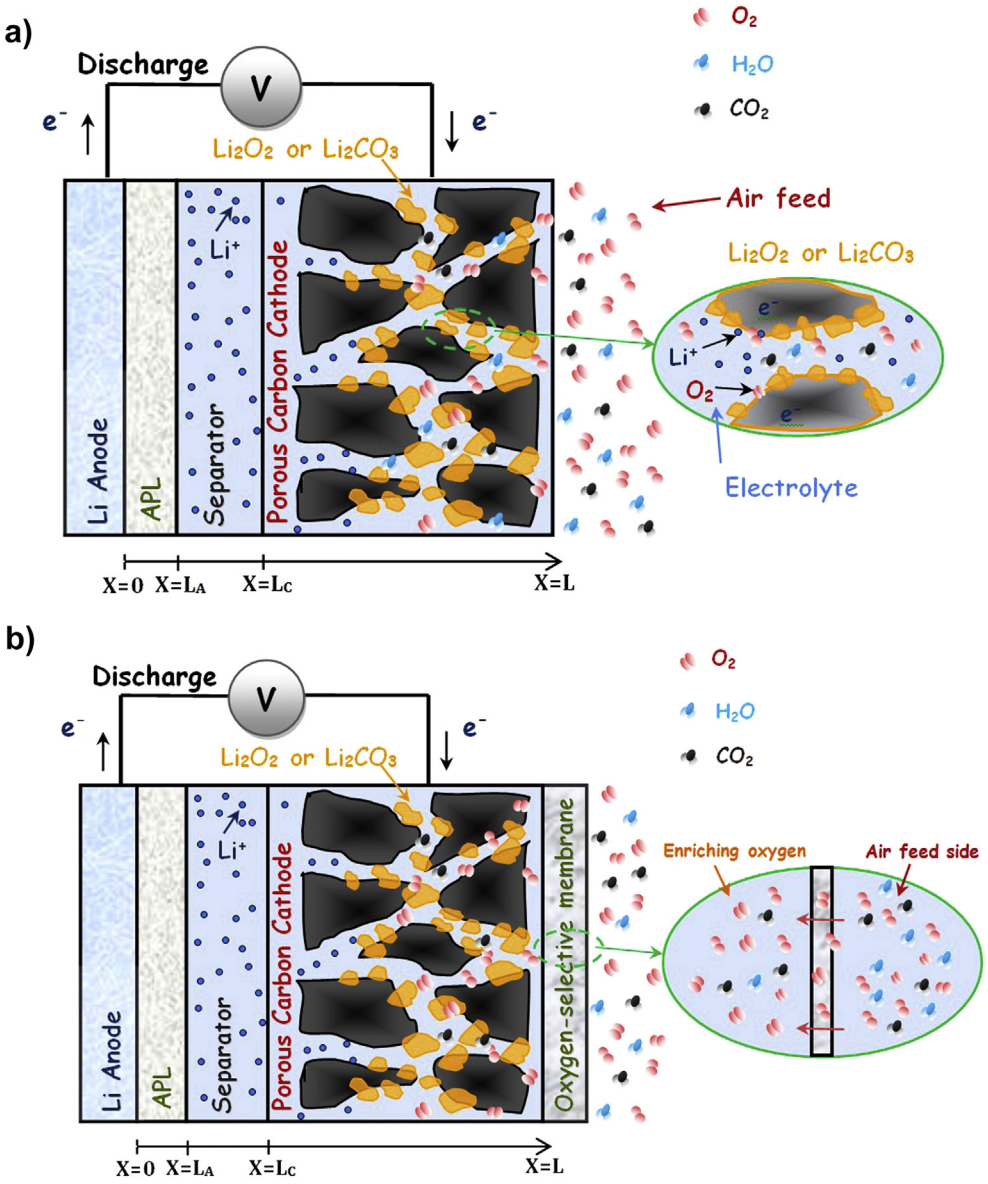

Fig. 1. Schematic computation domain of a Li-air battery during discharge operation. (a) Li-air battery operated with ambient air feeding and the inset demonstrates the discharge products formation of Li_2O_2 and Li_2CO_3 covering on the porous carbon surface. (b) Li-air battery protected by an oxygen-selective membrane at the cathode.

solvents is higher than oxygen [23]. This high solubility of CO_2 into the electrolyte could affect the Li-air performance due to the formation of Li_2CO_3.

Hence, unlike our previous model using only pure oxygen as feeding condition, the present model applied the air condition with low solubility of oxygen and CO_2. These concentrations in the porous cathode can affect the Li-air performance during battery cycling. Nitrogen also accesses through the cathode but has a little or no effect with lithium-based electrolyte on the Li-air battery performance [24].

2.2. Electrolyte degradation

In order to succeed in the application of non-aqueous Li-air batteries, finding of electrolytes with high stability during cell operation is a prerequisite for long-cycled life of Li-air battery, especially in an oxygen-rich environment and catalytic condition [25]. Since the Li-air battery have been developed, there is still no proper electrolyte that can meet all of these requirements: 1) high stability during cell operation [12,18,26,27], 2) high boiling point (low evaporation), and 3) high oxygen solubility and diffusivity as well as less sensitive to moisture [28]. At present, various non-aqueous electrolytes have been widely examined and applied in Li-air batteries based on different types of solvents, e.g. carbonates, ethers, sulfoxides, nitriles and ionic liquid [29]. However, Li_2CO_3 formation from decomposition of electrolyte by $Li–O_2$ intermediates and products was also clearly detected inside the electrode during discharge from all electrolytes dissolved in different solvents [29]. Hence, the electrolyte degradation mechanisms proposed in previous work [15] are also included in the present model and reinstated as described below.

2.2.1. Li_2CO_3 formation

$$2O_2 + 2e^- \xrightarrow{k_{1a}} 2O_2^- \quad E^0 = 3.18 \tag{1a}$$

$$2O_2^- + 2CO_2 \xrightarrow{k_{1b}} C_2O_6^{2-} + O_2 \quad \text{RDS} \tag{1b}$$

Table 1
Henry's constants and calculated concentrations in non-aqueous at 25 °C.

Species	Henry's law constant ($mol\ m^{-3}\ atm^{-1}$)	Concentration ($mol\ m^{-3}$)	Ref.
O_2	2.95	0.6182	Calculated from Ref. [47]
CO_2	4.59	0.0043	[48]

$$C_2O_6^{2-} + 4Li^+ + 2O_2^- \rightarrow 2Li_2CO_3 + 2O_2 \quad (1c)$$

$$\textbf{Overall}\quad 4Li^+ + 2CO_2 + 2O_2^- + 2e^- \rightarrow 2Li_2CO_3 + O_2 \quad E^0 = 7.19 \quad (IV)$$

2.2.2. Solvent degradation

$$O_2 + e^- \xrightarrow{k_{1a}} O_2^- \quad E^0 = 3.18 \quad (2a)$$

$$O_2^- + [\text{Solvent}] \rightarrow [\text{Solvent}]^- \quad (2b)$$

$$[\text{Solvent}]^- + O_2 \rightarrow CO_2 + H_2O + HCO_2Li + CH_3CO_2Li \quad (2c)$$

$$\textbf{Overall}\quad 2O_2 + [\text{Solvent}] + e^- \rightarrow CO_2 + H_2O + HCO_2Li + CH_3CO_2Li \quad (V)$$

It is worth noting that the exact details of the reaction routes for the electrolyte degradation to form Li_2CO_3 can be complicated regarding several intermediates during cell operation. Then, the proposed mechanisms above are a possibility to describe the formation reaction of Li_2CO_3 as reported previously [19,30,31].

With the use of air-feeding condition instead of favourite pure oxygen to the porous carbon cathode, the CO_2 in this model criterion could be generated from 2 routes, one from solvent or electrolyte degradation (Eq. (V)) and the other from the atmospheric air. Both Li_2O_2 and Li_2CO_3 can be produced as discharged products and are usually insoluble in the cell electrolyte. As a result, the repeated depositing film of different lithium salts over the carbon surface after each discharge and charge step affects the reaction mechanisms at the active area and electrolyte interfaces, and so the species transport inside the pores leading to cell voltage loss [32].

3. Battery model

3.1. Model description and assumptions

This work investigates the impacts of using air on a one-dimensional model for a prismatic single cell of a Li-air battery which constitutes of a thin lithium metal as negative electrode, an anode protective layer (APL), a porous separator soaked with non-aqueous electrolyte, and a porous carbon air cathode served as reaction site and accommodation for discharge products as shown in Fig. 1a. Current collectors are placed at the back of each electrode. The electrolytic solution is considered as a concentrated binary electrolyte to describe the motion for of each species in the systems. Due to the larger thickness of porous cathode than both of APL and separator, this area represents as the main contribution to influence the cell performance, thus we are particularly interested in analysing the effect of different parameters on the porous cathode for the Li-air simulation. The formation of solid products inside the porous cathode is based on a macro-homogeneous porous model defining the electrode by its porosity which is initially uniform but which dynamically changes as discharge occurs.

As the Li-air battery system is complex with the various reactions and mass transport species along the entire cell, the build-up of Li_2O_2 and Li_2CO_3, and the change of porosity and interfacial surface area vary with time and space, several model assumptions were adopted to support the calculation as follow:

- The Li-air battery is operated in isothermal conditions so that the thermal effects are not considered
- The lithium salts of Li_2O_2 and Li_2CO_3 are the main discharge products which only occur and deposit inside the porous cathode.
- The electrolytes used in Li-air batteries are assumed a binary monovalent electrolyte which consists of a single salt in a homogeneous organic solvent mixture.
- The electrolyte behaviour is based on concentrated solution theory to simulate the Li^+ diffusion.
- The pores in the cathode are filled of liquid phase electrolyte such as a solution of lithium hexafluorophosphate ($LiPF_6$) or lithium bistrifluoromethanesulfonamide (LiTFSI) in a non-aqueous solvent.
- The dried air feeding is assumed to dissolve as the concentration in the organic electrolyte with a saturated initial concentration so that no gas phase is occurred in the system.
- Convection for mass transport is negligible inside the cell.

3.2. Governing equations

The Li-air model applied in this work is based on previously developed literature in micro-macro homogeneous model for electrochemical cell system and Li-air battery [14,15]. This section provides the governing equations which describe conservation of mass and current, species transport, and reaction kinetic in the porous cathode and separator to clarify the mechanism inside the Li-air battery with ambient air operation.

3.2.1. Transport of species

As the model is based on the macroscopic theory of porous electrode which considers the solution and solid matrix phases as superimposed continuum [33,34]. Based on this approach, a material balance equation for species i transport in the Li-air electrolyte can be expressed as

$$\frac{\partial(\varepsilon c_i)}{\partial t} = -\nabla \cdot \boldsymbol{N}_i + r_i \quad (2)$$

where c_i is the bulk concentration of species i in the solution phase which is averaged over the volume of the solution in the pores, ε is the porosity of the electrode which is the electrolyte space in the matrix phase, $\boldsymbol{N}_i$ is the molar flux of species i in the porous solution averaged over the cross sectional area of the electrode, and r_i is the volumetric production rate of species i from the solid phase (electrode material) to solution phase (electrolyte in the porous) within the porous electrode.

The concentration of lithium salt electrolyte is the same as concentration of Li^+ due to the binary electrolyte assumption. Without convection, the diffusion and migration fluxes equations for mass transfer of Li^+ and all of the species transporting in the porous cathode can be expressed as

$$\boldsymbol{N}_{Li} = -D_{Li,eff}\nabla c_{Li} + \frac{\boldsymbol{i}_2 t_+}{F} \quad (3)$$

$$\boldsymbol{N}_i = -D_{i,eff}\nabla c_i \quad (4)$$

where $D_{Li,eff}$ and $D_{i,eff}$ are the effective diffusion coefficient of Li^+ and species i, respectively, t_+ is the transference number of Li^+, F is

Faraday's constant which is equal to 96,485 C mol^{-1}, and $\boldsymbol{i}_2$ is the current density in the solution phase or electrolyte current density which can be defined by the gradient of the potential in a 1:1 binary concentrated electrolyte solution as [33,35]

$$\boldsymbol{i}_2 = -\kappa_{\text{eff}}\nabla\phi_2 - \frac{2RT\kappa_{\text{eff}}}{F}(t_+ - 1)\left(1 + \frac{\partial \ln f}{\partial \ln c_{\text{Li}}}\right)\nabla \ln c_{\text{Li}} \quad (5)$$

where κ_{eff} is the effective conductivity of the electrolyte,ϕ_2 is the electrolyte potential (electric potential of Li^+), R is the universal gas constant which is equal to 8.3143 J mol^{-1} K^{-1}, T is the cell temperature in Kelvin, and f is the activity coefficient of $LiPF_6$ salt.

In the solid matrix phase, the movement of electron is governed by Ohm's law which evaluates the electric potential variation or potential of electron, ϕ_1, as follow

$$\boldsymbol{i}_1 = -\sigma_{\text{eff}}\nabla\phi_1 \quad (6)$$

where σ_{eff} is the effective conductivity of the electron in the electrode. This parameter is affected by the volume fraction of solid electrode inside the porous cathode.

Due to the tortuosity of porous cathode, the effective parameters of $D_{i,\text{eff}}$, κ_{eff} and σ_{eff} in the above equations are affected by the change of solid volume fraction and porosity (assigned as variable ε in the model) inside the porous medium. These parameters are applied for only the porous cathode region (others are not porosity) and are corrected to account for the porosity effect using Bruggeman correlation [36]

$$D_{\text{Li,eff}} = \varepsilon^{1.5} D_{\text{Li}} \quad (7)$$

$$D_{i,\text{eff}} = \varepsilon^{1.5} D_i \quad (8)$$

$$\kappa_{\text{eff}} = \varepsilon^{1.5}\kappa \quad (9)$$

$$\sigma_{\text{eff}} = (1-\varepsilon)^{1.5}\sigma \quad (10)$$

where D_{Li}, D_i, κ and σ are the diffusion coefficient of the Li^+ and each specie in electrolyte and the conductivity of electrolyte and electron in the cathode, respectively.

3.2.2. Conservation of charge

For the porous electrode theory, the charge conservation for the matrix and solution phases would require the divergence of the total current density to be zero defined by

$$\nabla\cdot\boldsymbol{i}_1 + \nabla\cdot\boldsymbol{i}_2 = 0 \quad (11)$$

During discharge or charge, the electrochemical reactions occurring at the electrode/electrolyte interface (charges transfer reaction) are expressed for individual reactions according to the conventionally general formula of the form

$$\sum s_i M_i^{z_i} \rightarrow n e^- \quad (12)$$

The charge transfer from solid phase to electrolyte phase per unit volume of electrode ($\nabla\cdot\boldsymbol{i}_2$) is related to the individual average transfer current density occurred at the cathode given by

$$\nabla\cdot\boldsymbol{i}_2 = \sum_m a j_m \quad (13)$$

This equation states that the transfer current per unit electrode volume is equivalent to the electrode chemical reaction rate where the M_i is a species symbol participating in the electrochemical reaction, z_i and s_i are the charge number and the stoichiometric coefficient of the species i, n is the number of electron transferred in the reaction, a is the specific interfacial area of the pore per unit volume of the total electrode, and j_m is local transfer current density between electrode and electrolyte interface of each reaction at the cathode. The value of s_i, z_i, and n can be defined by matching with an individual electrode reaction using the general form of Eq. (12), for example, the value of s_{Li}, z_{Li}, and n of Li^+ from Eq. (II) are −2, 1, and 2, respectively.

In practical Li-air cell, the precise reaction routes can be complicated regarding several intermediates as proposed in the previous reports [12,19]. Hence, both electrochemical reactions of Li_2O_2 and Li_2CO_3 formation inside porous electrode are considered in the present work. The superficial production rate of each species (referred to Eq. (2)) from solid phase to pore solution in the individual reactions m is given by Faraday's law

$$r_i = -\sum_m \frac{a s_{i,\text{m}}}{nF} j_m \quad (14)$$

3.3. Rate expression at cathode

The actual reaction paths and mechanisms for the discharge products are not available and quite complex involving various intermediates. Hence, to describe the electrochemical kinetic expression for the porous cathode, the model adopts the kinetic expression based on Eq. (II) for Li_2O_2 formation and on Eq. (V) for Li_2CO_3 formation.

3.3.1. Li_2O_2 formation

For electrochemical reaction of Li_2O_2 at the cathode, a modified version of the Butler–Volmer equation is applied in the model using two rate coefficients. The reaction for Li_2O_2 formation presented in Eq. (II) also depends on the concentration of Li^+ and oxygen for discharge and the concentration of Li_2O_2 during charge as in the following equation

$$\frac{j_{\text{II}}}{2F} = k_{\text{a}}(c_{\text{Li}_2\text{O}_2})\exp\left[\frac{(1-\beta)nF}{RT}\eta_m\right] - k_{\text{c}}(c_{\text{Li}^+})^2(c_{\text{O}_2})\exp\left[\frac{-\beta nF}{RT}\eta_m\right] \quad (15)$$

$$\eta_m = \phi_1 - \phi_2 - \Delta\phi_{\text{film}} - E_{\text{m}}^0 \quad (16)$$

$$\Delta\phi_{\text{film}} = j_c R_{\text{film}}\varepsilon_{\text{s}} \quad (17)$$

where k_{a} and k_{c} are the anodic and cathodic rate constant, respectively, β is the symmetry factor equal to 0.5, η_m is surface or activated overpotential for individual reaction, m, at the cathode, $\Delta\phi_{\text{film}}$ and R_{film} are the voltage drop and the electrical resistivity across Li_2O_2 film formation, respectively, ε_{s} is the volume fraction of solid formation of discharge products of Li_2O_2 and Li_2CO_3, and E_{m}^0 is the theoretical open-circuit potential for each reaction.

3.3.2. Li_2CO_3 formation

From our previous work [15], we proposed 2 mechanisms for Li_2CO_3 formation, one generated from reaction between superoxide and CO_2 (Eq. (IV)) and the other from the CO_2 reduction reaction. Because preliminary simulated results showed that the Li_2CO_3 formation from the latter demonstrated the insignificant value compared to the former, this model includes only one Li_2CO_3 formation mechanism. As explained before, the Li_2CO_3 formation is one of the discharge by-products coexisting with Li_2O_2. Thus, the decomposition of electrolyte, which initially forms CO_2 and finally

Table 2
Parameters used in simulation.

Parameter	Value	Unit	Symbol	Ref.
Cell properties				
Thickness of APL	5×10^{-8}	m	L_A	[11]
Thickness of separator	5×10^{-5}	m	L_C	[11]
Thickness of porous positive electrode	7.5×10^{-4}	m	L	[11]
Conductivity of positive electrode	10	S m^{-1}	σ	[49]
Porosity	0.73	–	ε^o	[50]
Specific interfacial area of cathode	3.75×10^6	m^2 m^{-3}	a	Calculated
Electrical resistivity across Li_2O_2 film formation	50	Ω m^2	R_{film}	[51]
Electrolyte properties				
Electrolyte concentration	1000	mol m^{-3}	$c_{Li,0}$	[7]
Li^+ diffusion coefficient[a]	2.11×10^{-9}	m^2 s^{-1}	D_{Li}	[52]
Oxygen diffusion coefficient	7×10^{-10}	m^2 s^{-1}	D_{O_2}	[47]
Superoxide diffusion coefficient	9×10^{-10}	m^2 s^{-1}	$D_{O_2^-}$	[53]
Carbon dioxide diffusion coefficient	1×10^{-9}	m^2 s^{-1}	D_{CO_2}	[31]
Conductivity of Li^+ in electrolyte	1.085	S m^{-1}	κ	[54]
Transference number of Li^+[a]	0.2594	–	t_+	[55]
$\partial lnf/(\partial lnc_{Li})$[a]	−1.03	–	–	[55]
Kinetic parameters				
Reaction rate coefficient anodic current	1.11×10^{-15}	m s^{-1}	k_a	Assumed
Reaction rate coefficient cathodic current	3.4×10^{-17}	m^7 s^{-1} mol^{-2}	k_c	Assumed
Reaction rate coefficient for O_2^- formation	8.1×10^{-15}	m s^{-1}	k_{1a}	Assumed
Reaction rate coefficient for Li_2CO_3 formation	370	m^3 s^{-1} mol^{-2}	k_{1b}	[31]
Reaction rate constant of CO_2 formation	5.9×10^{-15}	m s^{-1}	k_V	[56]
Exchange current density for anode	1	A m^{-2}	i_0	Assumed
Symmetry factor	0.5	–	β	[49]
General parameter				
Mass density of Lithium peroxide (Li_2O_2)	2140	kg m^{-3}	$\rho_{Li_2O_2}$	[57]
Mass density of electrolyte solution ($LiPF_6$)	1200	kg m^{-3}	ρ_{LiPF_6}	[57]
Mass density of Lithium carbonate (Li_2CO_3)	2110	kg m^{-3}	$\rho_{Li_2CO_3}$	[57]
Mass density of carbon	2260	kg m^{-3}	ρ_c	[57]
Operating temperature	298.15	K	T	

[a] Vary with concentration.

generates Li_2CO_3 as described above, occurs during Li-air operation. Some of the elementary steps in the electrolyte degradation sequences that lead to these by-products may be irreversible and non-electrochemical, so that the overall kinetic expression is very complex. Therefore, we use the kinetics for Li_2CO_3 formation on Eq. (IV) above based on the published kinetic data.

First the superoxide radical anion (O_2^-) that is initially formed (Eq. (1a)) during Li-air discharge as evidenced in previous study [37], attacks CO_2 which is generated from solvent decomposition (from Eq. (V)) to finally form Li_2CO_3 with the presence of Li^+ as follow reaction

$$j_{1a} = Fk_{1a}(c_{O_2})\left[-\exp\left(\frac{-\beta nF}{RT}\eta_m\right)\right] \quad (18)$$

$$r_{1b} = k_{1b}\left(c_{O_2^-}\right)(c_{CO_2}) \quad (19)$$

where k_{1a} and k_{1b} are the rate constant for the electrochemical reaction to form O_2^- and chemical reaction to generate Li_2CO_3, respectively. We use the Tafel form in Eq. (18) rather than the Butler–Volmer because the large kinetic overpotential during cell discharge puts the reaction in the Tafel region and considers only discharge (irreversible for O_2^- formation). It has been demonstrated that the chemical reaction in Eq. (19) is found to be first-order with to respect to both O_2^- with CO_2 reactants and is the rate determining step (RDS) [31]. Hence, the other reaction is considered as equilibrium and the formation of Li_2CO_3 can be predicted by using Eqs. (18) and (19) together.

3.3.3. Solvent degradation

The CO_2 generation can be created from the electrolyte degradation which is first attacked by the superoxide formation as described in Eq. (V). Apart from this decomposition, some reports demonstrate that side reactions to form CO_2 were observed at the cathode and were attributed to carbon decomposition during charge process [29,38]. However, only the CO_2 generated from electrolyte degradation will be considered here. Addressing this kinetic expression, because a detailed mechanism is not available, the CO_2 formation based on the overall reaction in Eq. (V), which consider the solvent concentration as constant is:

$$j_V = Fk_V(c_{O_2})\left[-\exp\left(\frac{-\beta nF}{RT}\eta_m\right)\right] \quad (20)$$

where k_V is the rate constant for the electrochemical reaction to form CO_2 and the others are the same as described above.

3.4. Rate expression at anode

The electrochemical reaction rate for the anode includes the oxidation of lithium metal to soluble Li^+. It is described by a general Butler–Volmer equation as follow

$$j_a = i_0\left[\exp\left(\frac{(1-\beta)nF}{RT}\eta_a\right) - \exp\left(\frac{-\beta nF}{RT}\eta_a\right)\right] \quad (21)$$

where i_0 is exchange current density for anode, η_a is surface or activated overpotential for reaction at anode, and the other parameter are as described above.

3.5. Specific surface area and porosity change

The specific area (a) of the electrode/electrolyte interface in Eq. (22) is decreased by the morphology and dynamic change of the porosity due to the solid discharge products of Li_2O_2 and Li_2CO_3.

These products are insoluble in several non-aqueous electrolytes and cover the active surface area during battery discharging. The variation of effective local surface area per unit volume of electrode can be commonly written by a geometric relation [39,40]

$$a = a_o\left[1 - \left(\frac{\varepsilon_s}{\varepsilon^o}\right)^p\right] \quad (22)$$

where ε_s and ε^o are the volume fraction of discharge products of Li_2O_2 and Li_2CO_3 solid, and initial electrode porosity, respectively. This empirical equation is used to describe the change in the interfacial area for electrochemical reactions that occur during discharge because of the fast passivation of Li_2O_2 and Li_2CO_3 covering a portion of the active sites for electrochemical reaction over the carbon surface [41]. The magnitude of exponent p is a geometrical factor indicating the morphology shape of the solid products that cover the active area. Small values of p indicate that the flat, plate-like precipitate shape of solid, conversely, large values of p reflects the needle-like solid which cover small active area. In this model, the value of 0.4 has been used.

The porosity volume change of the carbon electrode will be decreased due to the formation of insoluble solid products covering the catalyst and active particles as described in Eq (23). Thus, the effective conductivities and diffusivities for both Li^+ and all the species inside the porous cathode are affected by the porosity change. This can be described by the Bruggeman relationship (referred to Eqs. (7)–(10)). Because the solid distributions in the model are Li_2O_2 and Li_2CO_3, we use the properties of these solids for all of the discharge products formed on the individual reaction m

$$\frac{\partial \varepsilon}{\partial t} = \sum_{\text{solid phase } m} a j_m \frac{M_m}{nF\rho_m} \quad (23)$$

The volume fraction of the discharge solid formation can be determined from the cathode volume balance as

$$\varepsilon_s = 1 - \varepsilon - \varepsilon^o \quad (24)$$

where M_m and ρ_m are the molecular weight and the mass density of solid discharge products, respectively.

3.6. Initial conditions

To solve the governing equation for the battery cycling process, initial conditions are specified for all the species concentration inside the electrochemical cell, the porosity, the specific interfacial area, and the cell thickness. These initial values applied in the Li-air battery model are adopted from literature and summarised in Table 2. Before starting the discharge battery, the concentration for each species is assumed to uniformly distribute at all locations inside the cell system and equals to their initial concentration. Because the thickness of the porous cathode is much larger than both of APL and separator, then this area is regarded as the critical region of the computational domain affecting the cell performance.

3.7. Boundary conditions

From Fig. 1a, a schematic view of the model cell consists of four boundaries and three domain regions. Contrary to previous model, the constant for oxygen concentration feeding at the right side of the cathode ($x = L$) can be estimated form partial pressure using Henry's law constant as described above. At the current collector or the back side of the cathode electrode ($x = L$), the current density in the solid phase is equal to the applied discharge current density, the current density in the electrolyte phase equals to zero, and the flux of each species is zero. At the cathode electrode/separator interface ($x = L_c$) the continuous boundary conditions are specified for the fluxes of all species. The current density in the solid phase in this interface becomes zero, and the current density in the electrolyte then equals to the applied discharge current density. The voltage of the cell is calculated by the difference between the electrode potential at cathode current collector and the electrolyte potential at the anode side, $V_{cell} = \phi_1(x = L) - \phi_2(x = 0)$.

The conservation equations and the boundary conditions described above were discretized using a finite element method and solved in one-dimensional battery system by commercial software package COMSOL multiphysics version 4.3. The COMSOL software is designed to solve a set of coupled differential and algebraic equations. The battery simulation model is performed on a 32 bit Windows platform with 4GB RAM, and Intel Core 2 Duo 2.93 GHz processor. The different transport equations and the electrochemical reactions were solved as time dependent until the cell voltage reached the stop condition. The solution was considered as converged solution when the difference between two results was less than 10^{-4} (relative tolerance) for all variables.

4. Results and discussion

The one-dimensional Li-air battery implemented with the model equations as presented in the previous section have been simulated and solved to analyse the impact of using ambient air condition which is a severe effects on Li-air batteries comparing to the case of pure oxygen. As mentioned before, this model was based on previous work created by the author and could be validated by using the experimental cycle performance obtained in our labs, due to sufficient rechargeable data. In this section, first, the Li-air battery is considered the effects of using dried air only without those from electrolyte degradation to distinguish between these two mechanisms. Then, the model is combined the two effects together to investigate the cell performance in term of discharge specific capacity and Li_2CO_3 accumulation on cycling resulting in electrode passivation and capacity fading.

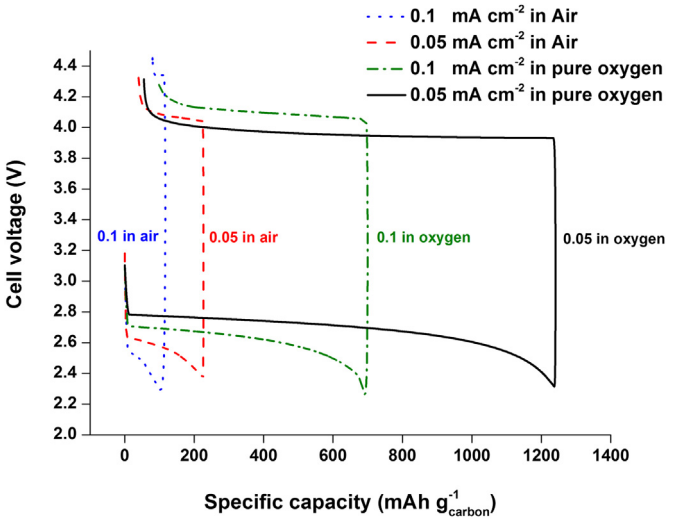

Fig. 2. Comparison of the voltage–capacity curve for a non-aqueous Li-air battery model in different feeding conditions between pure oxygen and ambient air at two operating rates of 0.05 and 0.1 mA cm^{-2}. The electrolyte contains 1 M $LiPF_6$ dissolved in acetonitrile. The cathode electrode thickness is 750 μm with porosity of 0.73. The cell cycle is simulated between 2.4 and 4.2 V versus Li/Li^+ in at operating temperature 298.15 K.

4.1. Li-air performance with air feeding

To compare the effect of using air into the Li-air battery, all parameters applied in the model are summarised in Table 2 and the oxygen and CO_2 concentrations in dried air are applied by following the atmospheric condition with low partial pressure as presented in Table 1. This model section excludes the effect from electrolyte degradation and considers the effect from air feeding only. The voltage–capacity results on 1st cycle obtained from the cell at different discharge rates are presented in Fig. 2. It is apparent that at the high discharge rate of 0.1 mA cm^{-2} there is a significant decrease in cell discharge capacity provided only 117 mAh g_{carbon}^{-1} when using air as the active reactant unlike the cell performance in pure oxygen providing the first discharge capacity around 700 mAh g_{carbon}^{-1} at the same discharge rate. A large deterioration of cell capacity can be attributed to the very low oxygen solubility in electrolyte at partial pressure 0.21 atm (0.618 mol m^{-3} compared to pure oxygen of 3.264 mol m^{-3} at 1 atm) and high discharge rate resulted in limited oxygen diffusion in the porous cathode. The CO_2 concentration which is even low solubility than that of oxygen could not much affect the cell capacity from Li_2CO_3 formation on 1st cycle.

Because the cell performance provided the low capacity at high discharge rate and could not determine the cell cycling behaviour, the discharge rate in the model was changed to lower value as 0.05 mA cm^{-2} to investigate the air effect compared to the pure oxygen at the same cycling rate as also presented in Fig. 2. It is apparent from the graph that although the battery capacity increases on changing the discharge rate, there has been a clear reduction of capacity from 1240 to 226 mAh g_{carbon}^{-1} when using ambient air as the feeding. What is also interesting in this data is that the inlet air affected not only the cell capacity but also the discharge voltage decreasing from 2.75 V in pure oxygen to 2.55 V in air at the same discharge rate. The cell performance is depleted because the oxygen substantially reduces in diffusion and solubility farther inside the porous structure when a Li-air battery operated in ambient condition. Moreover, the cycling profile of Li-air battery in Fig. 3 indicates that the discharge voltage slightly drops due to gradual Li_2CO_3 deposition when repeatedly cycles the Li-air battery. Because the electrolyte degradation effect is not include in this model section to clarify the ambient air effect only, then the battery

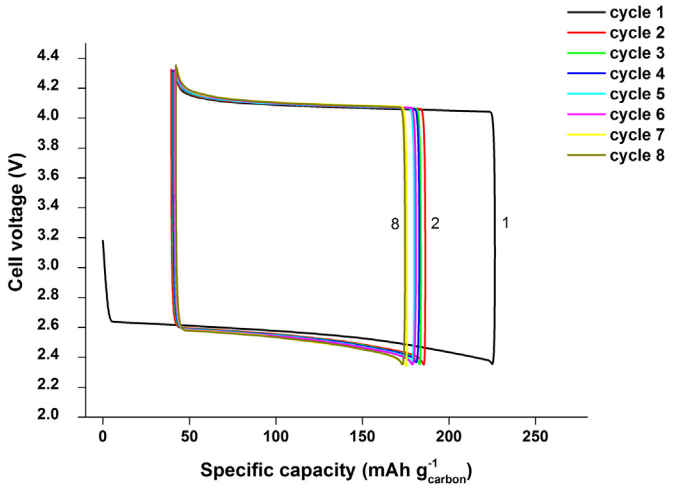

Fig. 3. Variation of voltage–capacity curve for a non-aqueous Li-air battery using ambient air in 8 cycles on discharge and then charge between 2.2 and 4.2 V versus Li/Li^+ at a rate of 0.05 mA cm^{-2}. The other parameters used in the model are the same as described in Fig. 2.

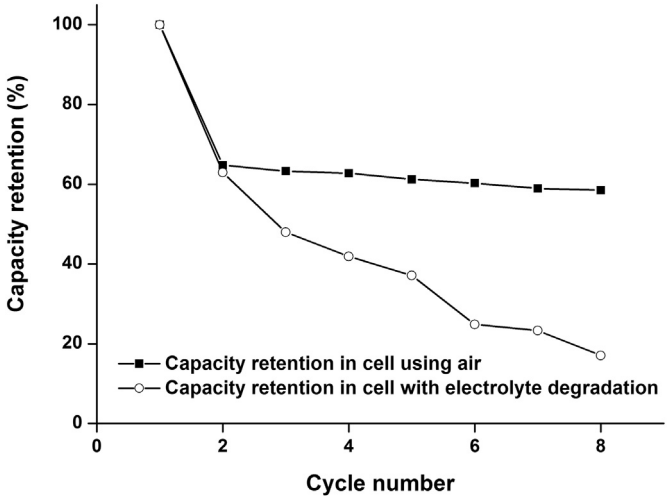

Fig. 4. The cycle performance in term of capacity retention of 8-cycle rechargeable Li-air battery in ambient air feeding compared between the cells with stabilised electrolyte and with electrolyte degradation effect. Battery was cycled at a rate 0.05 mA cm^{-2}. The other parameters used in the model are the same as described in Fig. 2.

profile between 2nd–8th cycle in Fig. 3 shows slightly decrease in specific capacity due to small Li_2CO_3 generated from low CO_2 concentration in air. The combining effects of air and electrolyte degradation will present in the next section.

The capacity retention of Li-air at a rate of 0.05 mA cm^{-2} is presented in Fig. 4, when the cell is operated by using an air inlet. The graph shows that the capacity retention gradually falls from 100% in the 1st cycle (cell discharge capacity of 226 mAh g_{carbon}^{-1}) to 65% in 2nd cycle and slightly decreases afterwards to 58% in 8th cycle. The significant difference of capacity retention between 1st and 2nd cycle is due to incompletely reversible Li_2O_2 during the recharging cell after 1st discharge. Thereafter, the cell is affected by the Li_2CO_3 formation (generated from Eq. (IV)) and demonstrates a small decrease of capacity retention during the cycling due to little contaminated CO_2. As can be seen from Table 3, the volume fraction of Li_2CO_3 collected at cathode/current collector interface at the end of each discharge cycle slightly increases and gradually deposits inside the cathode with the repeated cycle of the Li-air battery. This volume fraction is also plotted in Fig. 5 but the value is unnoticeable due to the scale when compared to Li_2CO_3 formation from the Li-air model including the electrolyte degradation effect, which will be described in the next section. Because the Li_2CO_3 formation tends

Table 3
Specific discharge capacity and Li_2CO_3 formation for a non-aqueous Li-air battery operated in ambient air in 8 cycles at a rate of 0.05 mA cm^{-2}. The data were compared between the cell with stabilised electrolyte and with electrolyte degradation effect.

Cycle	Discharge capacity (mAh g_{carbon}^{-1})		Capacity retention (%)		Li_2CO_3 volume fraction	
	Feeding air	With ED[a]	Feeding air	With ED[a]	Feeding air	With ED[a]
1	226.65	250.47	100.00	100.00	0.0031	0.0431
2	146.84	157.70	64.79	62.96	0.0072	0.0812
3	143.44	120.10	63.29	47.95	0.0108	0.1095
4	142.26	104.90	62.77	41.88	0.0143	0.1390
5	138.74	93.02	61.21	37.14	0.0178	0.1674
6	136.57	62.27	60.25	24.86	0.0212	0.1875
7	133.63	58.35	58.96	23.30	0.0245	0.2078
8	132.58	42.74	58.49	17.06	0.0277	0.2232

[a] Li-air battery performance combining the effect of feeding air and electrolyte degradation.

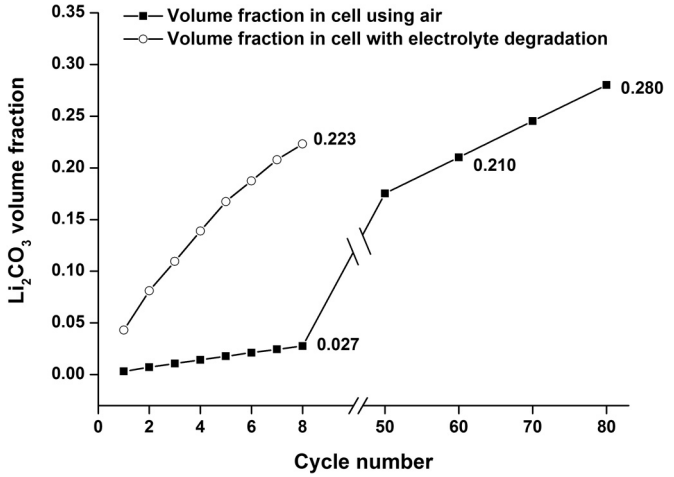

Fig. 5. Volume fraction of Li_2CO_3 formation inside the Li-air battery at the end of each discharge cycle compared between the cells with stabilised electrolyte and with electrolyte degradation effect. The parameters used in the model are the same as described in Fig. 2.

to follow the straight line during the cell simulation of 8-repeated cycle, then the cell can estimate how many cycles will achieve until the Li_2CO_3 deposition show significant impact on the Li-air cycling. Fig. 5 also provides the predicted Li_2CO_3 volume fraction extended to the 80th cycle, corresponding to the value of 0.28. In other words, when the Li-air battery is operated by using ambient air with stabilised electrolyte or without electrolyte degradation, it can be repeated discharge and charge to about 60–65 cycles before Li_2CO_3 formation reaches the same value as in the case of Li-air battery combining with electrolyte degradation effect giving only 8 cycles as compared in Fig. 5.

The evidence from this study indicates that the air feeding affects the cell performance in term of decreasing capacity due to the low diffusion and solubility of oxygen, but this ambient air operation does not impact much for the Li_2CO_3 generation during short-term cycles (8 cycles) due to limited CO_2 contamination from atmosphere.

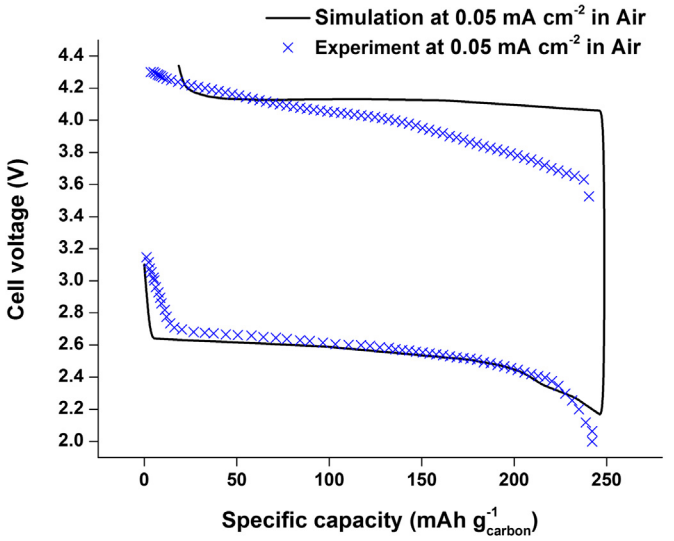

Fig. 6. Voltage–capacity curve for a non-aqueous Li-air battery operated in ambient air feeding on 1st cycle validated with our group experiment at a rate of 0.05 mA cm^{-2}. The electrolyte contains 1 M LiTFSI dissolved in TEGDME. The cell cycle is simulated between 2.4 and 4.2 V versus Li/Li$^+$ and both results are tested at operating temperature 298.15 K.

4.2. Comparing the Li-air model with experiment using air feeding

As previous section demonstrates the Li-air battery performance in various discharge rates on ambient air feeding without being compared to the real system, the developed model in this section is now validated against our group experimental data owning to sufficient and accessible information on Li-air battery. The result of 1st cycle obtained from the Li-air battery assembled in our lab is compared with the simulation as shown in Fig. 6. The air electrode was prepared by loading 3.54 mg cm^{-2} of Super P (Timcal, surface area 61 m^2 g^{-1}) without using any catalyst. The electrolyte loaded in the electrochemical cell and applied in the simulation for this section only was a 1 M lithium bis-trifluoromethanesulfonyl imide (LiTFSI) in tetraethylene glycol dimethyl ether (TEGDME or tetraglyme). It can be seen from the graph that the cell voltage–capacity curve at a rate of 0.05 mA cm^{-2} from the model matches well to the experimental data during cell operation in 1 atm of dry atmospheric air. During discharge, the cell potential fell steeply at the beginning, from a voltage of 3.1 V to a plateau at around 2.6 V which was in good agreement with the Li-air test cell for similar electrolyte and operating conditions. The Li-air model continuously discharged until reaching the cut-off voltage at 2.2 V corresponding to the discharge capacity based on the weight of carbon alone at 248 mAh g^{-1}_{carbon}, whereas the real system provided the discharge performance at 242 mAh g^{-1}_{carbon}. The validation of this study indicates that the developed Li-air model with the air feeding parameters can be used as a modelling tool to predict the Li-air battery performance in ambient condition. Contrary to expectations, the charging profile for the Li-air model did not fit well closely to the experiment cell at the commencement of the charging process as demonstrated in Fig. 6. The former started to charge at 4.0 V and maintained at this potential until the end of charging step, while the latter begin at 3.6 V and gradually increased to the same cut-off charging voltage at 4.3 V. The most likely cause of different in charging potential between the two results is that the Li_2O_2 formed on the first discharge of the Li-air battery with tetraglyme based solvent is coexisted with a mixture of Li_2CO_3, HCO_2Li, CH_3CO_2Li, and esters, due to electrolyte decomposition [19]. These products were not included for charging process in the case of Li-air battery model which considered only the Li_2O_2 as the truly rechargeable product. Hence, the charging potential of experimental cell may be vary according to the quantity of discharge products other than Li_2O_2. Moreover, the charge potential and capacity from both experiment and simulation demonstrated the same amount. This comparison confirms that the model results and experimental data show similarities and the model is a promising tool to identify the Li-air battery mechanisms and forecast the cell performance in ambient air.

4.3. Li-air performance combining the electrolyte degradation effect

In previous section, the model demonstrates only the effect air feeding into the Li-air battery to study the impact of using air on performance. However, in practical Li-air the challenge in non-aqueous electrolyte degradation still remains during battery operation and the formation of Li_2CO_3 is unavoidable. Since the Li-air battery is still in its early developing period, there is no electrolyte that is perfectly compatible to Li-air battery without electrolyte degradation. Hence, the model is combined electrolyte degradation effect together with air operation. As summarised in Table 3, the key results obtained from cycling Li-air battery with electrolyte degradation are compared with the cell using air feeding and also plotted in Figs. 4 and 5 in term of capacity retention and Li_2CO_3 formation, respectively. It is apparent that the discharge capacity decreases dramatically during cell cycling from 250 mAh g^{-1}_{carbon} in

the 1st cycle to very low value of 43 in the 8th cycle due to the high amount of irreversible Li_2CO_3 deposition as present in Fig. 5. This cell performance falls faster than the Li-air with stable electrolyte as the latter can maintain the discharge capacity to 132 mAh g_{carbon}^{-1} at the same cycle (see Table 3). The capacity retention (decreasing to 17% in 8th cycle) from the cell with electrolyte decomposition also follows the same trend of discharge capacity as shown in Fig. 4.

From this study, the electrolyte could be considered as a key component and one of the main issues to be solved at present to sustain the rechargeability of non-aqueous Li-air batteries. It needs to stable in both oxygen rich electrochemical condition during Li-air operation and intermediate-reduced species as well as the lithium oxides (LiO_x) compounds forming on discharge. Fundamentally, the stable electrolyte determines a desired discharge product (Li_2O_2) and whether a truly rechargeable Li-air battery can be built or not, i.e., high coulomb efficiency during each cycle is close to 99% to maintain battery cycle life. It is worth noting that although the electrolyte degradation in this model did not base on a detailed mechanism which includes complex elementary steps in the reaction sequence [12,19], the generic Li_2CO_3 formation reaction could be adequate to predict the Li-air deterioration during cycling.

4.4. Li-air performance with oxygen-selective membrane

As one mechanism for Li_2CO_3 formation and the hydrolysis reaction of the metallic lithium anode result from the cathode exposed to CO_2 and H_2O respectively from ambient air, it is necessary to prevent these gases entering to the Li-air battery. For example, the outer surface of the porous cathode could be covered with an oxygen diffusion membrane that may not only provide a much larger solubility of oxygen concentration through the membrane but also block CO_2 and moisture content from atmosphere [16,17]. Moreover, the membrane could also minimise the evaporation of electrolyte from the Li-air battery. In this section, the developed model considers the Li-air performance with the using of membrane as both an oxygen-selective medium to obtain a better discharge capacity and a CO_2 barrier to decrease the Li_2CO_3 formation. As shown in Fig. 1b, the porous cathode of Li-air battery is protected by the oxygen selective membrane facing the atmosphere. From the previous section, the Li-air battery including electrolyte decomposition effect tends to have higher Li_2CO_3 formation than the cell with the impact of CO_2 from atmosphere alone. Hence, to distinguish these effects when the Li-air battery integrates membrane, the electrolyte degradation effect is excluded in this section.

A membrane could be simply considered as an interphase barrier covering the Li-air porous cathode and used for the separation of ambient air into oxygen-enriching steam diffusing through the Li-air battery. The separation for each gas in membranes occurs due to different physical properties in term of permeability and solubility of the species flowing through the membrane. In this section, the Li-air model will be integrated with the silicone oil as an oxygen-selective liquid membrane for improving cell performance operated in ambient air. As mentioned early, the immobilized silicone oil membrane loaded in the various porous support films have been conducted in the Li-air batteries enabling to operate in ambient air with better performance [17]. To describe the mechanism of species in membrane, a simplified development of the theory of gas transport across a membrane is presented. For the single gas specie, several assumptions will be made to simplify the model and the diffusion of gas through the membrane can be defined by Fick's first law

$$N_{i,m} = -D_{i,m}\frac{dc_i}{dx} \tag{25}$$

where $N_{i,m}$ is the diffusion flux of gas through the membrane, $D_{i,m}$ is the diffusion coefficient in the membrane medium, and dc_i/dx is the concentration gradient of the gas across the membrane. If the diffusion flux does not change with time, a steady-state condition exists. Hence, the diffusion of gases through a membrane for which the concentrations of the diffusing species on both sides of a membrane are held constant. For a very thin membrane, if $D_{i,m}$ is assumed to be constant, Eq. (25) can be rearranged to

$$N_{i,m} = D_{i,m}\frac{(c_i - c_{i,m})}{l} \tag{26}$$

where c_i and $c_{i,m}$ are the concentration of the gas on upstream (air side) and downstream (after pass membrane), respectively, and l is the thickness of the membrane. For the membrane characterisation, the air or species permeation can be measured with the following equation

$$P_i = \frac{\overline{F}_i}{A_m \Delta\overline{p}_{i,g}} = \frac{N_{i,m}}{\Delta\overline{p}_{i,g}} \tag{27}$$

where $\overline{F}_i$ is the permeation flow rate of gas i (mol s^{-1}), A_m is the membrane surface area (m^2), and $\Delta\overline{p}_{i,g}$ is the partial pressure differential of gas i (Pa). By combining Eqs. (26) and (27) together, we can determine the concentration of gases after passing the membrane. To date various oxygen-selective membranes have been developed and laminated on the porous cathode to allow the unpressurised air permeating through the membranes, i.e. no pressure is applied at the upstream side of the membrane. The several assumptions are made to simplify the calculation: 1) the different partial pressures of individual gases between the two side of the membrane covered the surface of Li-air battery are not know unlike the membrane-testing cell that can be directly measured by pressure gauge, hence we assume this value as low as possible, 2) the diffusion coefficients of species in the thin membrane are assumed to be constant. The membrane characterisation and gases permeability for use in the Li-air battery with oxygen-selective membrane model are summarised in Table 4.

The Li-air performance obtained from the air-feeding cell integrated with the 50 μm thickness of silicone oil membrane is compared with the absence one as demonstrated in Fig. 7. Although, the membrane can enrich the oxygen concentration from 0.62 mol m^{-3} in air to 2.18 mol m^{-3} after passing the membrane, this is still not enough to operate the Li-air battery at high discharge rate. Hence, the low discharge rate at 0.05 mA cm^{-2} is applied in this section. As shown in Fig. 7, the silicone oil membrane with a relatively high oxygen permeability of 2×10^{-7} mol m^{-2} s^{-1} Pa^{-1} (oxygen concentration 2.18 mol m^{-3}) at room temperature enabled the Li-air batteries with porous electrode to operate in ambient air with a specific capacity of 796 mAh g_{carbon}^{-1}, 3.5 times higher than the case of without using membrane due to higher oxygen concentration. This discharge capacity obtained from the model is

Table 4
The membrane characterisation and gases permeability.

Membrane properties[a]	Value	Ref.
Thickness (m)	5×10^{-5}	[17]
Oxygen permeability (mol m^{-2} s^{-1} Pa^{-1})	2×10^{-7}	[43]
Carbon dioxide permeability (mol m^{-2} s^{-1} Pa^{-1})	1.08×10^{-6}	[43]
Oxygen diffusion coefficient in membrane (m^2 s^{-1})	1.6×10^{-9}	[43]
Carbon dioxide diffusion coefficient in membrane (m^2 s^{-1})	1.1×10^{-9}	[43]

[a] The membrane used in the model consists of silicone oil as the main material.

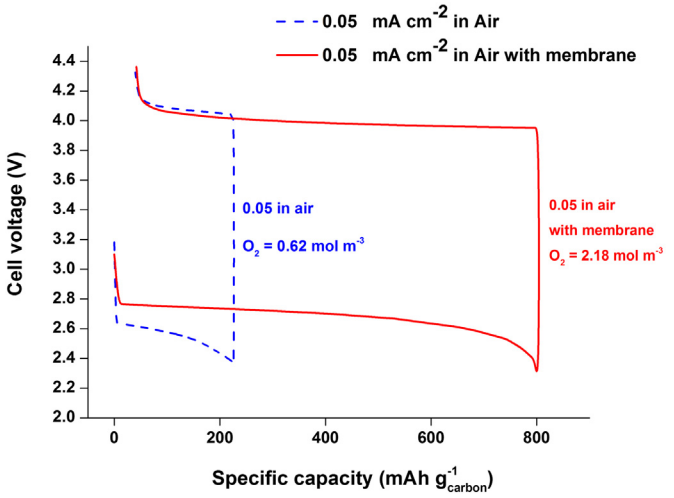

Fig. 7. Comparison of the voltage–capacity curve for a non-aqueous Li-air battery model operated in ambient air in the case with and without oxygen-selective membrane at a rate of 0.05 mA cm^{-2}. The other parameters used in the model are the same as described in Fig. 2.

similar to that obtained from the Li-air battery experiment using silicone oil liquid membrane for operation in ambient air, corresponding to a specific capacity of 789 mAh g^{-1}_{carbon} [17]. Moreover, it is apparent from the graph that the discharge cell voltages also increased, from ca. 2.60 V to 2.75 V with the higher dissolved oxygen concentration in the cell with membrane but the charging voltage did not affect much due to constant Li_2O_2 concentration which is assumed as the main product during battery charging. The CO_2 concentration also increased after permeation through the membrane owing to the higher permeability of CO_2 in silicone oil than oxygen (Table 4). However, the Li_2CO_3 generated from this increasing CO_2 did not notably influence the Li-air performance on the 1st cycle when comparing the enhancement of specific capacity.

4.5. Membrane with high oxygen permeability

One of the most significant properties of the membrane for attainment in superior Li-air performance in term of high capacity and discharge rate is the high oxygen permeability. In this section, the effect of oxygen permeability in various ranges on maximum discharge capacity at different rates is presented for a 50 μm thick membrane. The data were calculated using the equations as derived in previous section. This assumes that the air window on the membrane and the cathode electrode have equal geometric areas. The maximum specific discharge capacity at different rates for a Li-air battery limited by oxygen transport through an oxygen-selective membrane of any permeability can be compared in Fig. 8. It is apparent from the graphs that the specific capacity enhances with high oxygen permeability and it becomes smaller at higher discharge currents due to the limitation of the oxygen to diffuse inside the cathode. However, even with the high oxygen-permeable membrane the maximum discharge current to perform a Li-air battery is only 0.5 mA cm^{-2} with discharge capacity below 300 mAh g^{-1}_{carbon}. The results of this study indicate that although the specific capacity of Li-air batteries about two times higher than in conventional Li-ion batteries (150 mAh g^{-1}_{carbon}), the operating discharge currents are still not high enough for use in heavy-duty power devices or electric vehicles which require higher discharge rate.

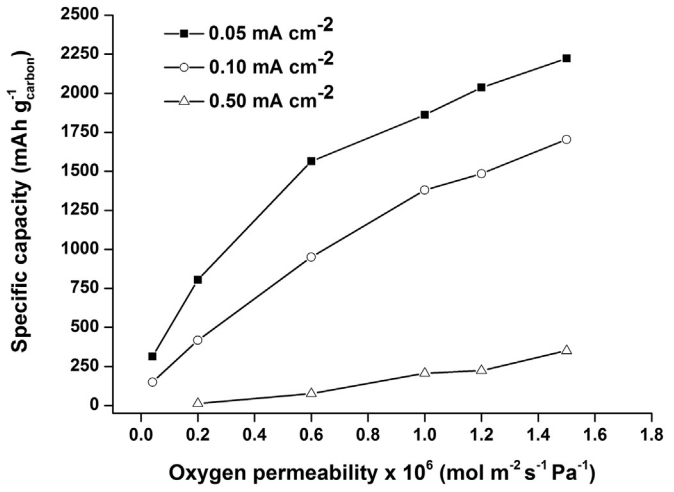

Fig. 8. Effect of oxygen permeability on maximum specific discharge capacity at different discharge rates of a non-aqueous Li-air battery protected with a 50 μm thick oxygen-selective membrane. The other parameters used in the model are the same as described in Fig. 2.

For CO_2 transport through most oxygen-selective membranes, its permeability is often comparable to oxygen, i.e. ratios of P_{O_2}/P_{CO_2} are generally less than unity [24]. CO_2 from atmosphere can react with the desired Li_2O_2 discharge product or electrolytes to form Li_2CO_3. The former product can reversibly charge to evolve oxygen at about 4.0–4.5 V lower than the latter which requires high potential more than 4.5 V to recharge [12,42]. Hence, if the membrane is being used for a rechargeable Li-air battery, it must effectively separate the CO_2 from the air inlet for maintaining a long-life cycle of Li-air battery. This is a challenge task because materials with high oxygen permeability also have high CO_2 permeability [43,44]. However, the CO_2 impurity is not the problem in primary Li-air batteries due to the absence of charging process so the final discharge product does not matter.

Nitrogen is inert gas and has a little or no effect with lithium-based electrolyte on the Li-air battery performance [24]. There are the published studies describe Lithium nitride (Li_3N) formation generated from the direct reaction of nitrogen with lithium at electrode in lithium ion batteries at room temperature during charge–discharge cycles [45,46]. The same behaviour could possibly occur on the surface of metallic lithium in Li-air battery. However, in this work we focus on the porous cathode which contributes to the main part of Li-air battery. Moreover, the permeability ratios between oxygen and nitrogen (P_{O_2}/P_{N_2}) are normally >1 thus increasing the relative oxygen over nitrogen in the feeding steam.

5. Conclusions

A macro-homogeneous model was developed and used to analyse the capacity and cycling behaviour of the rechargeable Li-air battery operated under ambient air conditions. The model uses a set of governing equations which describe species transport, charge and reaction kinetics within the battery, taking into consideration of by-product formation, electrolyte decomposition and changes in surface area and porosity. The model can accurately predict the capacity feature and the detrimental effect of electrolyte decomposition and Li_2CO_3 formation on the capacity retention. The model forecasts a significant influence of using an oxygen-selective membrane, which could lead to up to 4 times increment in specific capacity. The simulating results are in a good agreement with the experimental data.

Acknowledgements

The authors would like to thank the Ministry of Science and Technology, Royal Thai Government for funding Ukrit

Sahapatsombut PhD research and to the UK EPSRC for funding under grant number EP/I022570/1.

Nomenclature

a	specific interfacial area ($m^2\ m^{-3}$)
A_m	membrane surface area (m^2)
c_i	concentration of species i (mol m^{-3})
D_i	diffusion coefficient of species i ($m^2\ s^{-1}$)
$D_{i,eff}$	effective diffusion coefficient of species i ($m^2\ s^{-1}$)
E	electrode potential of cathode at any state (V)
E^0	electrode potential of cathode at standard state (V)
f	activity coefficient of $LiPF_6$ salt
F	Faraday's constant (96,485 C mol^{-1})
$\overline{F}$	permeation flow rate of gasses (mol s^{-1})
H	Henry's law constant
i_1	current density in the electrode phase ($A\ m^{-2}$)
i_2	current density in the electrolyte phase ($A\ m^{-2}$)
j	interfacial transfer current density of reaction m ($A\ m^{-2}$)
k	reaction rate constant
l	thickness of membrane (m)
L_A, L_C, L	thickness of APL, separator, and porous cathode respectively (m)
M_i	symbol for the chemical formula or molecular weight of species i (mol kg^{-1})
n	number of electrons transferred in the electrode reaction
N_i	molar flux of species i (mol $m^{-2}\ s^{-1}$)
p	surface effect factor
$\overline{p}$	partial pressure of gases (Pa)
P	Permeability of gasses (mol $m^{-2}\ s^{-1}\ Pa^{-1}$)
r_i	reaction rate term that accounts for electrochemical and chemical reactions (mol $m^{-3}\ s^{-1}$)
R	universal gas constant (8.3143 J $mol^{-1}\ K^{-1}$)
R_{film}	electrical resistivity across Li_2O_2 film formation ($\Omega\ m^2$)
s_i	stoichiometric coefficient of species i in electrode reaction
t	time (s)
t_+	transference number of cation in electrolyte
T	temperature (K)
V_{cell}	cell voltage (V)
z_i	valence of charge number of species i

Greek letters

α	transfer coefficient
β	symmetry factor
ε	porosity or void volume fraction of porous cathode
ε_s	volume fraction of solid phase in porous cathode
η	surface or activated overpotential (V)
κ	conductivity of electrolyte (S m^{-1})
κ_{eff}	effective conductivity of electrolyte (S m^{-1})
ν	number of moles of ions into which a mole of electrolyte dissociates
ν_+	numbers of moles of cations produced by the dissociation of a mole of electrolyte
ρ_i	density of a solid phase of species i ($kg\ m^{-3}$)
σ	conductivity of the electrode (S m^{-1})
σ_{eff}	effective conductivity of the electrode (S m^{-1})
ϕ_1	electric potential in the electrode (V)
ϕ_2	electric potential in the electrolyte (V)
$\Delta\phi_{film}$	voltage drop across Li_2O_2 film formation (V)
∇	differential operator

Subscripts and superscripts

o	initial
1	electrode phase
2	electrolyte phase
a	anodic
c	cathodic
g	gases
m	electrode reaction, solid species or membrane

References

[1] P.G. Bruce, S.A. Freunberger, L.J. Hardwick, J.M. Tarascon, Nat. Mater. 11 (2012) 19–29.
[2] J. Christensen, P. Albertus, R.S. Sanchez-Carrera, T. Lohmann, B. Kozinsky, R. Liedtke, J. Ahmed, A. Kojic, J. Electrochem. Soc. 159 (2012) R1–R30.
[3] G. Girishkumar, B. McCloskey, A.C. Luntz, S. Swanson, W. Wilcke, J. Phys. Chem. Lett. 1 (2010) 2193–2203.
[4] J.S. Lee, S.T. Kim, R. Cao, N.S. Choi, M. Liu, K.T. Lee, J. Cho, Adv. Energy Mater. 1 (2011) 34–50.
[5] K.M. Abraham, Z. Jiang, J. Electrochem. Soc. 143 (1996) 1–5.
[6] T. Ogasawara, A. Débart, M. Holzapfel, P. Novák, P.G. Bruce, J. Am. Chem. Soc. 128 (2006) 1390–1393.
[7] J. Read, J. Electrochem. Soc. 149 (2002) A1190–A1195.
[8] T. Kuboki, T. Okuyama, T. Ohsaki, N. Takami, J. Power Sourc. 146 (2005) 766–769.
[9] H. Cheng, K. Scott, J. Power Sourc. 195 (2010) 1370–1374.
[10] C.O. Laoire, S. Mukerjee, K.M. Abraham, E.J. Plichta, M.A. Hendrickson, J. Phys. Chem. C 114 (2010) 9178–9186.
[11] J.G. Zhang, D. Wang, W. Xu, J. Xiao, R.E. Williford, J. Power Sources 195 (2010) 4332–4337.
[12] S.A. Freunberger, Y. Chen, Z. Peng, J.M. Griffin, L.J. Hardwick, F. Bardé, P. Novák, P.G. Bruce, J. Am. Chem. Soc. 133 (2011) 8040–8047.
[13] W. Xu, V.V. Viswanathan, D. Wang, S.A. Towne, J. Xiao, Z. Nie, D. Hu, J.-G. Zhang, J. Power Sources 196 (2011) 3894–3899.
[14] U. Sahapatsombut, H. Cheng, K. Scott, J. Power Sources 227 (2013) 243–253.
[15] U. Sahapatsombut, H. Cheng, K. Scott, J. Power Sources 243 (2013) 409–418.
[16] J. Zhang, W. Xu, X. Li, W. Liu, J. Electrochem. Soc. 157 (2010) A940–A946.
[17] J. Zhang, W. Xu, W. Liu, J. Power Sources 195 (2010) 7438–7444.
[18] W. Xu, K. Xu, V.V. Viswanathan, S.A. Towne, J.S. Hardy, J. Xiao, Z. Nie, D. Hu, D. Wang, J.G. Zhang, J. Power Sources 196 (2011) 9631–9639.
[19] S.A. Freunberger, Y. Chen, N.E. Drewett, L.J. Hardwick, F. Bardé, P.G. Bruce, Angew. Chem. Int. Ed. 50 (2011) 8609–8613.
[20] K. Takechi, T. Shiga, T. Asaoka, Chem. Commun. 47 (2011) 3463–3465.
[21] D. Zhang, R. Li, T. Huang, A. Yu, J. Power Sources 195 (2010) 1202–1206.
[22] F.T. MacKenzie, Our Changing Planet: an Introduction to Earth System Science and Global Environmental Change, Prentice Hall, 2010.
[23] M. Jitaru, J. Univ. Chem. Technol. Metall. 42 (2007) 333–344.
[24] O. Crowther, M. Salomon, Membranes 2 (2012) 216–227.
[25] Y. Shao, F. Ding, J. Xiao, J. Zhang, W. Xu, S. Park, J.G. Zhang, Y. Wang, J. Liu, Adv. Funct. Mater. 23 (2013) 987–1004.
[26] B.D. McCloskey, D.S. Bethune, R.M. Shelby, G. Girishkumar, A.C. Luntz, J. Phys. Chem. Lett. 2 (2011) 1161–1166.
[27] F. Mizuno, S. Nakanishi, Y. Kotani, S. Yokoishi, I. Hideki, Electrochemistry 78 (2010) 403–405.
[28] Y. Wang, D. Zheng, X.Q. Yang, D. Qu, Energy Environ. Sci. 4 (2011) 3697–3702.
[29] W. Xu, J. Hu, M.H. Engelhard, S.A. Towne, J.S. Hardy, J. Xiao, J. Feng, M.Y. Hu, J. Zhang, F. Ding, M.E. Gross, J.G. Zhang, J. Power Sources 215 (2012) 240–247.
[30] J.L. Roberts Jr., T.S. Calderwood, D.T. Sawyer, J. Am. Chem. Soc. 106 (1984) 4667–4670.
[31] J.D. Wadhawan, P.J. Welford, E. Maisonhaute, V. Climent, N.S. Lawrence, R.G. Compton, H.B. McPeak, C.E.W. Hahn, J. Phys. Chem. B 105 (2001) 10659–10668.
[32] J. Xiao, J. Hu, D. Wang, D. Hu, W. Xu, G.L. Graff, Z. Nie, J. Liu, J.G. Zhang, J. Power Sources 196 (2011) 5674–5678.
[33] J. Newman, K.E. Thomas-Alyea, Electrochemical Systems, 3 ed., John Wiley & Sons, New York, 2004.
[34] J. Newman, W. Tiedemann, AIChE J. 21 (1975) 25–41.
[35] W.A.v . Schalkwijk, B. Scrosati, Advances in Lithium-ion Batteries, Kluwer Academic/Plenum Publishers, New York, 2002.
[36] D.A.G. Bruggeman, Ann. Phys. (Leipzig) 24 (1935) 636–679.
[37] Z. Peng, S.A. Freunberger, L.J. Hardwick, Y. Chen, V. Giordani, F. Bardé, P. Novák, D. Graham, J.M. Tarascon, P.G. Bruce, Angew. Chem. Int. Ed. 50 (2011) 6351–6355.
[38] M.M. Ottakam Thotiyl, S.A. Freunberger, Z. Peng, P.G. Bruce, J. Am. Chem. Soc. 135 (2013) 494–500.
[39] R.M. LaFollette, D.N. Bennion, J. Electrochem. Soc. 137 (1990) 3701–3707.
[40] C.Y. Wang, W.B. Gu, B.Y. Liaw, J. Electrochem. Soc. 145 (1998) 3407–3417.
[41] X. Ren, S.S. Zhang, D.T. Tran, J. Read, J. Mater. Chem. 21 (2011) 10118–10125.
[42] T. Zhang, H. Zhou, Nat. Commun. 4 (2013).
[43] W.L. Robb, Ann. N. Y. Acad. Sci. 146 (1968) 119–137.
[44] A.M.A. Dias, M. Freire, J.A.P. Coutinho, I.M. Marrucho, Fluid Phase Equilib. 222–223 (2004) 325–330.
[45] H. Wang, W.-D. Zhang, Z.-Q. Deng, M.-C. Chen, Solid State Ionics 180 (2009) 212–215.
[46] D.J. David, M.H. Froning, T.N. Wittberg, W.E. Moddeman, Appl. Surf. Sci. 7 (1981) 185–195.

[47] J. Read, K. Mutolo, M. Ervin, W. Behl, J. Wolfenstine, A. Driedger, D. Foster, J. Electrochem. Soc. 150 (2003) A1351–A1356.
[48] A. Gennaro, A.A. Isse, E. Vianello, J. Electroanal. Chem. Interfacial Electrochem. 289 (1990) 203–215.
[49] P. Andrei, J.P. Zheng, M. Hendrickson, E.J. Plichta, J. Electrochem. Soc. 157 (2010).
[50] Y.-C. Lu, D.G. Kwabi, K.P.C. Yao, J.R. Harding, J. Zhou, L. Zuin, Y. Shao-Horn, Energy Environ. Sci. 4 (2011) 2999–3007.
[51] Q. Li, H.Y. Sun, Y. Takeda, N. Imanishi, J. Yang, O. Yamamoto, J. Power Sources 94 (2001) 201–205.
[52] S.G. Stewart, J. Newman, J. Electrochem. Soc. 155 (2008) F13–F16.
[53] C.O. Laoire, S. Mukerjee, K.M. Abraham, E.J. Plichta, M.A. Hendrickson, J. Phys. Chem. C 113 (2009) 20127–20134.
[54] C.M. O'Laoire, in: Chemistry and Chemical Biology, Northeastern Universiy, Boston, Massachusetts, 2010.
[55] A. Nyman, M. Behm, G. Lindbergh, Electrochim. Acta 53 (2008) 6356–6365.
[56] P. Albertus, G. Girishkumar, B. McCloskey, R.S. Sánchez-Carrera, B. Kozinsky, J. Christensen, A.C. Luntz, J. Electrochem. Soc. 158 (2011) A343–A351.
[57] D.R. Lide, CRC Handbook of Chemistry and Physics, 87 ed., Taylor & Francis, Boca Raton, Florida, 2007.